Pré-Publicações do Departamento de Matemática
Universidade de Coimbra
Preprint Number 21–16

DENSITY-PRESSURE IBVP: NUMERICAL ANALYSIS, SIMULATION AND CELL DYNAMICS IN A COLONIC CRYPT

G.C.M. CAMPOS, J. A. FERREIRA AND G. ROMANAZZI

Abstract: This paper aims to propose a finite difference method for an differential-algebraic systems that couples an elliptic equation with a convection-diffusion-reaction equation with mixed derivatives. The parabolic equation depends on the gradient of the solution of the elliptic equation. If the numerical approximation for this gradient presents lower accuracy then the numerical approximations for the solution of the parabolic equation can be deteriorated. In order to get a second order approximation for the solution of the parabolic equation, the challenges that we have to face are the construction of the right discretizations of the elliptic and parabolic equations that lead to a second order approximation for the gradient as well as the development of the numerical analysis of the proposed method. Numerical simulations in the context of cell dynamics in a colonic crypt of the human colon will be presented.

Keywords: Coupled system of elliptic and parabolic equations, Mixed derivatives, Finite difference methods, Cell dynamics, Colonic crypt.

1. Introduction

This paper intents to propose a numerical method for the initial boundary value problem (IBVP)

$$\begin{cases} -\nabla\cdot(\mathcal{A}\nabla p) = \alpha c, \\ \dfrac{\partial c}{\partial t} + \nabla\cdot(v(\nabla p)c) = \nabla\cdot(D\mathcal{A}\nabla c) + \beta c, \quad \text{in } \Omega\times(0,T], \\ p = 0\,, c = 0 \,\text{on}\, \partial\Omega\times(0,T], \\ c(0) = c_0 \,\text{in}\,\Omega, \end{cases} \tag{1}$$

where $\Omega = (0,1)^2$, $\partial\Omega$ represents its boundary, T denotes a final time, $\mathcal{A}$ represents a matrix of order 2 with entries $\mathcal{A}_{ij}, i,j = 1,2$, α and β are bounded functions in $\overline{\Omega}$, $v : \mathbb{R}^2 \to \mathbb{R}^2$ with $v = (v_1, v_2)$, is such that $v_\ell : \mathbb{R}^2 \to \mathbb{R}, \ell = 1,2$, are bounded and Lipschitz functions, that is, there exists a positive constant L_v such that $|v_\ell(\mathbf{z}) - v_\ell(\tilde{\mathbf{z}})| \leq L_v\|\mathbf{z}-\tilde{\mathbf{z}}\|_2, \mathbf{z}, \tilde{\mathbf{z}} \in \mathbb{R}^2$. It should be pointed out that, for $\mathbf{z} \in \mathbb{R}^2$, $v(\mathbf{z})$ should be identified with $-A\mathbf{z}$ when

Received June 1, 2021.

$\|\mathbf{z}\|_\infty << +\infty$, and $\lim_{\|\mathbf{z}\|_\infty \to +\infty} \|v(\mathbf{z})\|_\infty = v_\infty < +\infty$. This last assumption means that the convective velocity $v(\nabla p)$ is bounded when $\|\nabla p\|_\infty \to +\infty$. Later, we take $v(\mathbf{z}) = -A\mathbf{z}, \mathbf{z} \in \mathbb{R}^2$ in the examples in Section 5 and $v(\mathbf{z}) = -\xi A\mathbf{z}$ in Section 6, where $\xi > 0$ is constant. We refer to c and p in (1) as concentration and pressure, respectively.

To solve numerically the IBVP (1) we can use the MOL (method of lines) approach: spatial discretization followed by a time integration. The spatial discretization converts the IBVP (1) in a differential-algebraic system - an ordinary differential system coupled with a system of algebraic equations. This system can be solved numerically using an efficient and accurate numerical method for this kind of problems (see for instance [2], [9]). We observe that the second equation of (1) depends on the gradient of p defined in the first equation. If such gradient is not computed with an adequate accuracy then the accuracy of the approximation for c can be lost. Our aim is to propose a finite difference method defined on nonuniform rectangular grids of Ω that presents truncation error of first order with respect to the norm $\|.\|_\infty$ but leads to a second order approximation for ∇p and for c.

We observe that (1) presents mixed derivatives. This fact leads to additional difficulties that were analyzed in [4] and [5]) for elliptic equations and the research in the numerical treatment of these type of derivatives have not been fruitful. Without being exhaustive we mention [3] where parabolic equations in high dimension space have been considered and high-order compact schemes where proposed defined in uniform partitions for each space component. In financial market Heston models have been proposed to describe the time evolution of European option prices that depend on the underlying asset price and its variance. These models are defined by a PDE presents the mixed derivative of the option price with respect the underlying asset price and its variance. A common approach to compute numerical approximations for the option prices in this case is to use a transformation of variables that eliminates the mixed derivative term in the new PDE that is defined in a new domain with a curved boundary. The treatment of the new problem using finite difference methods presents new difficulties associated with the spatial grid (see [8] and their references). In [7] the Heston-Hull-White PDE was discretized using centered finite difference operators in the original space domain for the underlying asset price, its variance and for the risk asset domains, considering nonuniform grids that are smooth transformations

of uniform partitions. No theoretical analysis was present in this work to support the obtained numerical results.

In this paper our aim is to propose a semi-discrete finite difference method (FDM) to compute approximations for the pressure p and concentration c defined by the IBVP (1). The FDM is considered in nonuniform rectangular grids and it leads to a second order approximation for p and c with respect to a discrete version of the usual H^1-norm. Particular attention will be given to (1) in the context of the cell dynamics in a colonic crypt of the human colon. The human colon is prone to develop a cancer due to its cell renovation that consists in a large number of cell divisions per day located in small cavities of the colon epithelium, called crypts. The colon epithelium is filled by millions of crypts, and it is known that mutations in the cell proliferation process (inside the crypts) can lead to the carcinogenesis. The model that governs the interactions between three populations of cells is a coupled PDE system formed by an elliptic and parabolic equations whose unknowns are the proliferative cell density c and the exerted cell pressure p.

The paper is organized as follows. In Section 2 we introduce notations and basic results. In Section 3 we present a first attempt to conclude the stability of the semi-discrete problem where we conclude that we need to impose the uniform boundness of the numerical gradient of p to get stability. This results is proved starting by establishing the uniform boundness of the semi-discrete approximations. The convergence analysis of the proposed semi-discrete approximation is established in Section 4. Section 5 is devoted to the numerical illustration of the convergence results established here and the numerical behavior of p and c in the context of the proliferative cell density and the exerted cell pressure in a human colonic crypt is the focus of Section 6. Finally, in Section 7 we present some conclusions.

2. Definition and preliminary results

Let $\Omega = (0,1)^2$ and Λ be a sequence of vectors $H = (h,k)$, $h = (h_1, \ldots, h_N), k = (k_1, \ldots, k_M)$ with positive entries satisfying $\sum_{i=1}^{N} h_i = \sum_{j=1}^{M} k_j = 1$. Let $H_{max} = \max\{h_{max}, k_{max}\}$ with $h_{max} = \max_{i=1,\ldots,N} h_i$ and $k_{max} = \max_{j=1,\ldots,M} k_j$. Analogously, we define $H_{min} = \min\{h_{min}, k_{min}\}$ with $h_{min} = \min_{i=1,\ldots,N} h_i$ and $k_{min} = \min_{j=1,\ldots,M} k_j$. We assume that $H_{max} \to 0$. For $H \in \Lambda$ we introduce in $\overline{\Omega} = [0,1]^2$

the spatial grid $\overline{\Omega}_H$ defined by

$$\begin{aligned}\overline{\Omega}_H = \ & \{(x_i, y_j), i = 0, \ldots, N, j = 0, \ldots, M, x_0 = y_0 = 0, x_N = y_M = 1, \\ & x_i = x_{i-1} + h_i, i = 1, \ldots, N, y_j = y_{j-1} + k_j\,, j = 1, \ldots, M\}.\end{aligned}$$

We introduce also the following sets

$$\partial\Omega_H = \overline{\Omega}_H \cap \partial\Omega,\ \Omega_H = \overline{\Omega}_H / \partial\Omega_H.$$

Let W_H be the vector space of grid function $u_H : \overline{\Omega}_H \to \mathbb{R}$. By $W_{H,0}$ we represent the subspace of W_H of the grid functions that are null on $\partial\Omega_H$ where we consider the following inner product

$$(v_H, w_H)_H = \sum_{i,j=1}^{N-1,M-1} h_{i+\frac{1}{2}} k_{j+\frac{1}{2}} v_H(x_i, y_j) w_H(x_i, y_j), v_H, w_H \in W_{H,0},$$

where $h_{i+\frac{1}{2}} = \dfrac{h_i + h_{i+1}}{2}$ being $k_{j+\frac{1}{2}}$ defined analogously. By $\|.\|_H$ we represent the norm induced by the last inner product.

We use the following notations: for $\mathbf{v}_H = (v_{H,1}, v_{H,2}), \mathbf{w}_H = (w_{H,1}, w_{H,2}) \in [W_H]^2$,

$$(\mathbf{v}_H, \mathbf{w}_H)_{H-} = (v_{H,1}, w_{H,1})_{h-} + (v_{H,2}, w_{H,2})_{k-},$$

with

$$(v_{H,1}, w_{H,1})_{h-} = \sum_{i,j=1}^{N,M-1} h_i k_{j+\frac{1}{2}} v_{H,1}(x_i, y_j) w_{H,1}(x_i, y_j)$$

being $(v_{H,2}, w_{H,2})_{k-}$ defined analogously.

We also introduce in $[W_H]^2$ the semi-norm

$$\|\mathbf{v}_H\|_{H-} = (\mathbf{v}_H, \mathbf{v}_H)_{H-}^{1/2} = \left(\|v_{H,1}\|_{h-}^2 + \|v_{H,2}\|_{k-}^2\right)^{1/2},$$

where $\|v_{H,1}\|_{h-}^2 = (v_{H,1}, v_{H,1})_{h-}$ and $\|v_{H,2}\|_{k-}^2$ is defined analogously.

By $\nabla_{H-} = (D_{-x}, D_{-y})$ we denote the discrete gradient where D_{-x}, D_{-y} are the backward finite difference operators in x, y-directions respectively. We introduce now in $W_{H,0}$ the following discrete version of the usual H^1-norm

$$\|v_H\|_{1,H} = \left(\|v_H\|_H^2 + \|\nabla_{H-} v_H\|_{H,-}^2\right)^{1/2},\ v_H \in W_{H,0}.$$

Let $D_x^\star$ be defined by

$$D_x^\star v_H(x_i, y_j) = \frac{v_H(x_{i+1}, y_j) - v_H(x_i, y_j)}{h_{i+\frac{1}{2}}},$$

being $D_y^\star$ defined analogously. By ∇_H^* we represent the following operator

$$\nabla_H^*.\mathbf{v}_H(x_i,y_j) = D_x^\star v_{H,1}(x_i,y_j) + D_y^\star v_{H,2}(x_i,y_j), (x_i,y_j) \in \Omega_H,$$

for $\mathbf{v}_H = (v_{H,1}, v_{H,2}) \in [W_H]^2$.

By $D_{c,x}$ we denote the first order centered operator with respect to x direction

$$D_{c,x}v_H(x_i,y_j) = \frac{v_H(x_{i+1},y_j) - v_H(x_{i-1},y_j)}{h_i + h_{i+1}},$$

being $D_{c,y}$ the correspondent first order centered operator with respect to y direction. Let $\nabla_c = (D_{c,x}, D_{c,y})$ be defined by

$$\nabla_c.\mathbf{v}_H(x_i,y_j) = D_{c,x}v_{H,1}(x_i,y_j) + D_{c,y}v_{H,2}(x_i,y_j),$$

and

$$\nabla_c v_H(x_i,y_j) = (D_{c,x}v_H(x_i,y_j), D_{c,y}v_H(x_i,y_j)),$$

for $(x_i,y_j) \in \Omega_H$ and $\mathbf{v}_H \in [W_H]^2, v_H \in W_{H,0}$.

We consider also the operator $D_H = (D_h, D_k)$ where

$$D_h v_H(x_i,y_j) = \frac{h_{i+1}D_{-x}v_H(x_i,y_j) + h_i D_{-x}v_H(x_{i+1},y_j)}{h_{i+1}+h_i},\ (x_i,y_j) \in \Omega_H,$$

for $v_H \in W_H$, being D_k defined analogously. We will use $D_h v_H(x_N,y_j) = D_{-x}v_H(x_N,y_j)$, $D_h v_H(x_0,y_j) = D_{-x}v_H(x_1,y_j)$, $D_k v_H(x_i,y_M) = D_{-y}v_H(x_i,y_M)$, and $D_k v_H(x_i,y_0) = D_{-y}v_H(x_i,y_1)$.

Finally by M_x we denote the average operator

$$M_x v_H(x_i,y_j) = \frac{1}{2}(v_H(x_i,y_j) + v_H(x_{i-1},y_j)), (x_i,y_j) \in \Omega_H,$$

being M_y defined analogously. This allows to define the operator $M_H : [W_H]^2 \to [W_H]^2$ as follows

$$M_H(\mathbf{v}_H)(x_i,y_j) = (M_x(v_{H,1})(x_i,y_j), M_y(v_{H,2})(x_i,y_j)), \mathbf{v}_H \in [W_H]^2.$$

In order to simplify the presentation, we also consider

$$\begin{array}{ll} M_x(x_i,y_j) = (\frac{1}{2}(x_i + x_{i-1}), y_j), & M_y(x_i,y_j) = (x_i, \frac{1}{2}(y_j + y_{j-1})) \\ a(M_x)(x_i,y_j) = a(M_x(x_i,y_j)), & a(M_y)(x_i,y_j) = a(M_y(x_i,y_j)), \end{array}$$

with $a : \overline{\Omega} \to \mathbb{R}$.

Proposition 2.1. *For all $v_H, w_H \in W_{H,0}$, $a : \overline{\Omega} \to \mathbb{R}$, we have*

$$\|M_x v_H\|_{h-} \leq \|v_H\|_H, \tag{2}$$

$$-(D_x^\star(a(M_x))D_{-x}v_H), w_H)_H = (a(M_x)D_{-x}v_H, D_{-x}w_H)_{h-}, \tag{3}$$

$$-(D_{c,x}v_H, w_H)_H = (v_H, D_{c,x}w_H)_H, \tag{4}$$

$$-(D_{c,x}v_H, w_H)_H = (M_x(v_H), D_{-x}w_H)_{h-}, \tag{5}$$

$$-(D_{c,x}(aD_{c,y}v_H), w_H)_H = (M_x(aD_{c,y}v_H), D_{-x}w_H)_{h-}, \tag{6}$$

$$-(D_{c,x}v_H, D_{c,y}v_H)_H \leq \|\nabla_{H-}v_H\|_{H-}^2, \tag{7}$$

$$\|D_h v_H\|_H \leq \sqrt{2}C_{g,h}\|D_{-x}v_H\|_{h-}, \tag{8}$$

$$\|v_H\|_H^2 \leq \frac{1}{2}\|\nabla_{H-}v_H\|_{H-}^2, \tag{9}$$

$$\|v_H\|_\infty^2 \leq \frac{1}{2}\|\nabla_{H-}v_H\|_{H-}^2, \tag{10}$$

where $\|v_H\|_\infty = \max_{(x,y)\in\Omega_H} |v_H(x,y)|$ *and* $\dfrac{h_{max}}{h_{min}} \leq C_{g,h}$.

Proof: The proof of (2)-(5) and (7)-(8), can be easily made by direct verification. The relation (6) follows from (5) replacing v_H by $aD_{c,y}v_H$, To prove (9) and (10) we observe that

$$v_H(x_i, y_j)^2 \leq \sum_{\ell=1}^{N} h_\ell (D_{-x}v_H(x_\ell, y_j))^2, (x_i, y_j) \in \Omega_H.$$

■

Inequality (9) is usually referred as discrete Poincaré-Friedrichs inequality. In what follows we use the following matrix norm

$$\|A\|_{C_b^m(\mathbb{R}^2)} = \max_{i,j=1,2} \|A_{ij}\|_{C_b^m(\mathbb{R}^2)},$$

where $C_b^m(\mathbb{R}^2)$ denotes the space of functions defined in $\mathbb{R}^2$ with bounded derivatives of order less or equal than $m \in \mathbb{N}_0$, and $\|A_{ij}\|_{C_b^m(\mathbb{R}^2)} = \max_{\ell=0,\ldots,m} \|A_{ij}^{(\ell)}\|_\infty$.

The semi-discrete approximation $p_H(t), c_H(t) \in W_{H,0}$ for the solution of the differential-algebraic IBVP (1) that we study in this work is defined by

the following differential-algebraic initial value problem (IVP)

$$\begin{cases} -\mathcal{L}_{\mathcal{A}} p_H(t) = \alpha c_H(t), \\ c_H'(t) + \nabla_c \cdot (c_H(t) v(D_H p_H(t))) = \mathcal{L}_{\mathcal{B}}(c_H(t)) + \beta c_H(t), \ \text{ in } \Omega_H, t \in (0,T], \\ p_H(t) = c_H(t) = 0, \ \text{ on } \partial\Omega_H, t \in (0,T], \\ c_H(0) = R_H c_0, \ \text{ in } \Omega_H. \end{cases} \tag{11}$$

In (11), $R_H : C(\overline{\Omega}) \to W_H$ denotes the restriction operator $R_H w(x_i, y_j) = w(x_i, y_j), (x_i, y_j) \in \overline{\Omega}_H, w \in C(\overline{\Omega})$, $\mathcal{L}_{\mathcal{A}}$ is the following finite difference operator

$$\begin{aligned} \mathcal{L}_{\mathcal{A}} v_H(x_i, y_j) = \ & \nabla^*_H . \Big(\begin{bmatrix} A_{11}(M_x) & 0 \\ 0 & A_{22}(M_y) \end{bmatrix} \nabla_{H-} v_H \Big)(x_i, y_j) \\ & + \nabla_c . \Big(\begin{bmatrix} 0 & A_{12} \\ A_{21} & 0 \end{bmatrix} \nabla_c v_H \Big)(x_i, y_j), \ (x_i, y_j) \in \Omega_H, v_H \in W_{H,0}, \end{aligned} \tag{12}$$

being the operator $\mathcal{L}_{\mathcal{B}}$ defined as $\mathcal{L}_{\mathcal{A}}$ with $\mathcal{A}$ replaced by $\mathcal{B} = D\mathcal{A}$.

Let $a_H(.,.) : [W_{H,0}]^2 \to \mathbb{R}$ be the bilinear form associated with the finite difference operator $-\mathcal{L}_{\mathcal{A}}$ defined by

$$\begin{aligned} a_H(u_H, w_H) = \ & (M_x(\mathcal{A}_{11}) D_{-x} u_H, D_{-x} w_h)_{h-} + (M_x(\mathcal{A}_{12} D_{c,y} u_H), D_{-x} w_h)_{h-} \\ & + (M_y(\mathcal{A}_{21} D_{c,x} u_H), D_{-y} w_h)_{k-} + (M_y(\mathcal{A}_{22}) D_{-y} u_H, D_{-y} w_h)_{k-}, \end{aligned}$$

for $u_H, w_H \in W_{H,0}$. In fact, it can be proved that

$$(-\mathcal{L}_{\mathcal{A}} u_H, w_H)_H = a_H(u_H, w_H), \quad u_H, w_H \in W_{H,0}, \tag{13}$$

by using (3) and (6).

In what follows we assume that $a_H(.,.)$ is elliptic, that is, there exists a positive constant $C_{e,a}$, H independent, such that

$$a_H(u_H, u_H) \geq C_{e,a} \|u_H\|^2_{1,H}, \ u_H \in W_{H,0}. \tag{14}$$

We assume also that the bilinear form $b_H(.,.) : [W_{H,0}]^2 \to \mathbb{R}$ associated with the finite difference operators $-\mathcal{L}_{\mathcal{B}}$, defined as $a_H(.,.)$ with $\mathcal{A}$ replaced by $\mathcal{B}$, is elliptic, that is, there exists a positive constant $C_{e,b}$, H independent, such that

$$b_H(u_H, u_H) \geq C_{e,b} \|u_H\|^2_{1,H}, \ u_H \in W_{H,0}. \tag{15}$$

It is clear that assuming convenient conditions on the entries of $\mathcal{A}$ and $\mathcal{B}$, it can be shown that (14) and (15) hold.

For instance for the term $(M_x(\mathcal{A}_{12}D_{c,y}u_H), D_{-x}w_h)_{h-}$ we have

$$\begin{aligned}
|(M_x(\mathcal{A}_{12}D_{c,y}u_H), D_{-x}u_h)_{h-}| &= \sum_{i=1}^{N}\sum_{j=1}^{M-1}\frac{h_i}{2}k_{j+1/2}\Big(|\mathcal{A}_{12}(x_i,y_j)||D_{c,y}u_H(x_i,y_j|)\\
&\quad +|\mathcal{A}_{12}(x_{i-1},y_j)||D_{c,y}u_H(x_{i-1},y_j)|\Big)|D_{-x}u_H(x_i,y_j)|\\
&\leq \frac{1}{\sqrt{2}}\|\mathcal{A}_{12}\|_\infty\Big(\sum_{i=1}^{N}\sum_{j=1}^{M-1}h_ik_{j+1/2}\Big(D_{c,y}u_H(x_i,y_j)^2\\
&\quad +D_{c,y}u_H(x_{i-1},y_j)^2\Big)\Big)^{1/2}\|D_{-x}u_H\|_{h-}\\
&\leq \frac{1}{\sqrt{2}}\|\mathcal{A}_{12}\|_\infty\Big(\sum_{i=1}^{N}\sum_{j=1}^{M-1}h_{i+1/2}2k_{j+1/2}D_{c,y}u_H(x_i,y_j)^2\Big)^{1/2}\|D_{-x}u_H\|_{h-}\\
&\leq \frac{1}{\sqrt{2}}\|\mathcal{A}_{12}\|_\infty\Big(\sum_{i=1}^{N-1}\sum_{j=1}^{M}2h_{i+1/2}k_jD_{-y}u_H(x_i,y_j)^2\Big)^{1/2}\|D_{-x}u_H\|_{h-}\\
&\leq \|\mathcal{A}_{12}\|_\infty\|D_{-y}u_H\|_{k-}\|D_{-x}u_H\|_{h-}.
\end{aligned}$$

Analogously, we also have

$$|(M_y(\mathcal{A}_{21}D_{c,x}u_H), D_{-x}w_h)_{h-}| \leq \|\mathcal{A}_{21}\|_\infty\|D_{-y}u_H\|_{k-}\|D_{-x}u_H\|_{h-}.$$

Then we obtain

$$\begin{aligned}
|(M_x(\mathcal{A}_{12}D_{c,y}u_H), D_{-x}w_h)_{h-}|+ \;& |(M_y(\mathcal{A}_{21}D_{c,x}u_H), D_{-y}w_h)_{k-}|\\
&\leq (\|\mathcal{A}_{12}\|_\infty + \|\mathcal{A}_{21}\|_\infty)\|D_{-y}u_H\|_{k-}\|D_{-x}u_H\|_{h-}.
\end{aligned}$$

It is clear that, if for instance,

$$\mathcal{A}_{ii} \geq \mathcal{A}_0 > 0\, i = 1, 2,$$

and

$$A_0 > \frac{1}{2}(\|\mathcal{A}_{12}\|_\infty + \|\mathcal{A}_{21}\|_\infty),$$

then (14) holds.

3. Stability of the semi-discrete differential-algebraic IVP

We study in what follows the stability of the differential- algebraic IVP (11). Here and in the following section we suppose that v is bounded and Lipschitz, and α, β are bounded functions in $\bar{\Omega}$. Let $c_H, \tilde{c}_H \in C^1([0,T], W_{H,0})$ solutions of this IVP with initial conditions $c_H(0), \tilde{c}_H(0) \in W_{H,0}$ and let $p_H(t), \tilde{p}_H(t)$ the corresponding pressures. We establish in what follows upper bounds for

$\|c_H(t) - \tilde{c}_H(t)\|_{1,H}$ and $\|p_H(t) - \tilde{p}_H(t)\|_{1,H}$. We start by studying $\|p(t)\|_{1,H}$ and $\|c_H(t)\|_{1,H}$.

Proposition 3.1. *Let $c_H \in C^1([0,T], W_{H,0})$ and $p_H(t) \in W_{H,0}$, $t \in (0,T]$, be defined by the differential algebraic IVP (11) with initial condition $c_H(0)$. If $a_H(.,.)$ and $b_H(.,.)$ are elliptic in $[W_{H,0}]^2$ with ellipticity constants $C_{e,a}$ and $C_{e,b}$, then*

$$\|p_H(t)\|_{1,H}^2 \leq \frac{\|\alpha\|_\infty^2}{C_{e,a}^2} e^{(\frac{\|v\|_\infty^2}{C_{e,b}} + 2\|\beta\|_\infty)t} \|c_H(0)\|_H^2, \tag{16}$$

and

$$\|c_H(t)\|_H^2 + C_{e,b} \int_0^t e^{(\frac{\|v\|_\infty^2}{C_{e,b}} + 2\|\beta\|_\infty)(t-s)} \|c_H(s)\|_{1,H}^2 ds \leq e^{(\frac{\|v\|_\infty^2}{C_{e,b}} + 2\|\beta\|_\infty)t} \|c_H(0)\|_H^2, \tag{17}$$

for $t \in [0,T]$.

Proof: From (11) and (13) we easily get

$$a_H(p_H(t), p_H(t)) = (\alpha c_H(t), p_H(t))_H \tag{18}$$

and using (5) we obtain

$$\begin{aligned} \frac{1}{2}\frac{d}{dt}\|c_H(t)\|_H^2 + b_H(c_H(t), c_H(t)) \; &= (M_H(c_H(t)v(D_H p_H(t))), \nabla_{H-} c_H(t))_{H-} \\ &\quad + \|\beta\|_\infty \|c_H(t)\|_H^2. \end{aligned} \tag{19}$$

Considering the ellipticity of $a_H(.,.)$ and (18) we establish

$$C_{e,a}\|p_H(t)\|_{1,H}^2 \leq \frac{\|\alpha\|_\infty^2}{4\varepsilon^2}\|c_H(t)\|_H^2 + \varepsilon^2 \|p_H(t)\|_H^2, \tag{20}$$

and, by using the ellipticity of $b_H(.,.)$ and the equations (2), (19), we get

$$\begin{aligned} \frac{1}{2}\frac{d}{dt}\|c_H(t)\|_H^2 + C_{e,b}\|c_H(t)\|_{1,H}^2 \; &\leq \frac{\|v\|_\infty^2}{4\eta^2}\|c_H(t)\|_H^2 + \eta^2 \|\nabla_{H-} c_H(t)\|_{H-}^2 \\ &\quad + \|\beta\|_\infty \|c_H(t)\|_H^2, \end{aligned} \tag{21}$$

where $\varepsilon, \eta \neq 0$ are arbitrary constants. Choosing, in (20) and (21), $\varepsilon^2 = \frac{1}{2}C_{e,a}$ and $\eta^2 = \frac{1}{2}C_{e,b}$, respectively, we get

$$\|p_H(t)\|_{1,H}^2 \leq \frac{\|\alpha\|_\infty^2}{C_{e,a}^2}\|c_H(t)\|_H^2 \tag{22}$$

and

$$\frac{d}{dt}\Big(\|c_H(t)\|_H^2 e^{-(\frac{\|v\|_\infty^2}{C_{e,b}}+2\|\beta\|_\infty)t} + C_{e,b}\int_0^t e^{-(\frac{\|v\|_\infty^2}{C_{e,b}}+2\|\beta\|_\infty)s}\|c_H(s)\|_{1,H}^2 ds\Big) \leq 0, \tag{23}$$

for $t \in (0,T]$.

Finally, inequalities (22) and (23) lead to (16) and (17). ■

Corollary 3.2. *Under the assumptions Proposition 3.1 holds the following*

$$\int_0^t \|c_H(s)\|_\infty^2 \leq \frac{1}{2C_{e,b}} e^{(\frac{\|v\|_\infty^2}{C_{e,b}}+2\|\beta\|_\infty)t}\|c_H(0)\|_H^2, t \in [0,T]. \tag{24}$$

Proof: It is enough to combine (17) with (10).

■

In the next result we establish upper bounds for $\omega_p(t)$ and $\omega_c(t)$.

Proposition 3.3. *Let $c_H, \tilde{c}_H \in C^1([0,T], W_{H,0})$ and $p_H(t), \tilde{p}_H(t) \in W_{H,0}$, $t \in (0,T]$, be defined by the differential algebraic IVP (11) with initial condition $c_H(0)$, $\tilde{c}_H(0)$, respectively. Let λ be a sequence of stepsizes such that there exists $C_g > 0$ satisfying*

$$\frac{H_{max}}{H_{min}} \leq C_g, \tag{25}$$

for $H \in \Lambda$ with H_{max} small enough.

If $a_H(.,.)$ and $b_H(.,.)$ are elliptic in $[W_{H,0}]^2$ with ellipticity constants $C_{e,a}$ and $C_{e,b}$, then for $\omega_c(t) = c_H(t) - \tilde{c}_H(t), \omega_p(t) = p_H(t) - \tilde{p}_H(t)$ and for $H \in \Lambda$ with H_{max} small enough, we have

$$\|\omega_p(t)\|_{1,H}^2 \leq \frac{\|\alpha\|_\infty^2}{C_{e,a}^2} e^{\int_0^t \left(\frac{4}{C_{e,b}}\left(\frac{4L_v^2C_g^2}{C_{e,a}^2}\|\alpha\|_\infty^2\|c_H(s)\|_\infty^2+\|v\|_\infty^2\right)+2\|\beta\|_\infty\right)ds} \|\omega_c(0)\|_H^2, \tag{26}$$

and

$$\|\omega_c(t)\|_H^2 + C_{e,b}\int_0^t e^{\int_s^t \left(\frac{4}{C_{e,b}}\left(\frac{4L_v^2C_g^2}{C_{e,a}^2}\|\alpha\|_\infty^2\|c_H(\mu)\|_\infty^2+\|v\|_\infty^2\right)+2\|\beta\|_\infty\right)d\mu}\|\omega_c(s)\|_{1,H}^2 ds \leq e^{\int_0^t \left(\frac{4}{C_{e,b}}\left(\frac{4L_v^2C_g^2}{C_{e,a}^2}\|\alpha\|_\infty^2\|c_H(s)\|_\infty^2+\|v\|_\infty^2\right)+2\|\beta\|_\infty\right)ds}\|\omega_c(0)\|_H^2, \tag{27}$$

for $t \in [0,T]$.

Proof: From (11) and (13) it can be shown that $\omega_c(t)$ and $\omega_p(t)$ satisfy the following

$$\|\omega_p(t)\|_{1,H}^2 \leq \frac{\alpha^2}{C_{e,a}^2}\|\omega_c(t)\|_H^2 \tag{28}$$

and, similarly to (19), we have

$$\begin{aligned}&\frac{1}{2}\frac{d}{dt}\|\omega_c(t)\|_H^2 + C_{e,b}\|\omega_c(t)\|_{1,H}^2\\ &\quad\leq (M_H\big(c_H(t)v(D_Hp_H(t)) - \tilde{c}_H(t)v(D_H\tilde{p}_H(t))\big), \nabla_{H-}\omega_c(t))_{H-}\\ &\quad+\|\beta\|_\infty\|\omega_c(t)\|_H^2.\end{aligned} \tag{29}$$

As for $\ell = 1, 2$, holds the following

$$\begin{aligned}c_H(t)v_\ell(D_Hp_H(t)) - \tilde{c}_H(t)v_\ell(D_H\tilde{p}_H(t)) = \;& c_H(t)(v_\ell(D_Hp_H(t)) - v_\ell(D_H\tilde{p}_H(t)))\\ &+v_\ell(D_H\tilde{p}_H(t))\omega_c(t),\end{aligned}$$

considering the assumption (25), the relations (2),(8), the Lipschitz property of v_ℓ and the upper bound (28), we get

$$\begin{aligned}(M_H\big(c_H(t)v(D_Hp_H(t)) - \tilde{c}_H(t)v(D_H\tilde{p}_H(t))\big), \nabla_{H-}\omega_c(t))_{H-}&\\ \leq \frac{2}{\eta^2}L_v^2C_g^2\|c_H(t)\|_\infty^2\|\nabla_{H-}\omega_p(t)\|_{H-}^2&\\ + \frac{1}{2\eta^2}\|v\|_\infty^2\|\omega_c(t)\|_H^2 + 2\eta^2\|\nabla_{H-}\omega_c(t)\|_{H-}^2 &\qquad (30)\\ \leq\big(\frac{2}{\eta^2}L_v^2C_g^2\frac{\|\alpha\|_\infty^2}{C_{e,a}^2}\|c_H(t)\|_\infty^2 + \frac{1}{2\eta^2}\|v\|_\infty^2\big)\|\omega_c(t)\|_H^2&\\ + 2\eta^2\|\nabla_{H-}\omega_c(t)\|_{H-}^2, &\qquad (31)\end{aligned}$$

where $\eta \neq 0$ is an arbitrary constant. Inserting in (29) the last upper bound and fixing $\eta^2 = \frac{1}{4}C_{e,b}$, we obtain

$$\begin{aligned}&\frac{d}{dt}\|\omega_c(t)\|_H^2 + C_{e,b}\|\omega_c(t)\|_{1,H}^2\\ &\quad\leq \Big(\frac{4}{C_{e,b}}\big(\frac{4L_v^2C_g^2}{C_{e,a}^2}\|\alpha\|_\infty^2\|c_H(t)\|_\infty^2 + \|v\|_\infty^2\big) + 2\|\beta\|_\infty\Big)\|\omega_c(t)\|_H^2.\end{aligned} \tag{32}$$

Inequality (32) leads to (27) and from (28) we conclude (26). ■

Finally Proposition 3.3 and Corollary 3.2 enable us to conclude the stability of the differential-algebraic IVP (11).

4. Convergence analysis

Let $e_c(t) = R_H c(t) - c_H(t)$ and $e_p(t) = R_H p(t) - p_H(t) \in W_{H,0}$ be the spatial discretization errors induced by the spatial discretization that defines the differential algebraic IVP (11). In these errors, $c_H(t)$ and $p_H(t)$ are solutions of the IVP (11). Let $T_{\mathcal{L}_\mathcal{A}}(t)$, $T_{\mathcal{L}_\mathcal{B}}(t)$ be the spatial truncation errors induced by the spatial discretizations defined by $\mathcal{L}_\mathcal{A}$, $\mathcal{L}_\mathcal{B}$ and let $T_{\nabla_c}(t)$ be the truncation error that arises from the discretization of $\nabla.(c(t)v(\nabla p(t)))$. We introduce $T_p(t) = T_{-\mathcal{L}_\mathcal{A}}(t)$ and $T_{c,p}(t) = T_{-\mathcal{L}_\mathcal{B}}(t) + T_{\nabla_c}(t)$. For the errors $e_c(t), e_p(t), T_p(t)$ and $T_{c,p}(t)$ we have

$$\begin{cases} -\mathcal{L}_\mathcal{A} e_p(t) = \alpha e_c(t) + T_p(t), \\ e_c'(t) + \nabla_c \cdot \left(R_H c(t) v(D_H R_H p(t)) - c_H(t) v(D_H p_H(t))\right) = \mathcal{L}_\mathcal{B}(e_c(t)) \\ \qquad\qquad +\beta e_c(t) + T_{c,p}(t), \ \text{ in } \Omega_H, t \in (0,T], \\ e_p(t) = e_c(t) = 0, \ \text{ on } \partial\Omega_H, t \in (0,T], \\ e_c(0) = 0 \ \text{ in } \Omega_H. \end{cases} \tag{33}$$

If $p(t) \in C^4(\overline{\Omega})$ then the truncation error $T_{\mathcal{L}_\mathcal{A}}(t)$ that admits the representation

$$T_{\mathcal{L}_\mathcal{A}}(t) = \mathcal{L}_\mathcal{A}(R_H p(t)) - R_H \nabla.(A \nabla p(t))$$

can be split into

$$T_{\mathcal{L}_\mathcal{A}}(t) = T^{(1)}_{\mathcal{L}_\mathcal{A}}(t) + T^{(2)}_{\mathcal{L}_\mathcal{A}}(t),$$

with

$$T^{(1)}_{\mathcal{L}_\mathcal{A}}(x_i, y_j, t) = (h_{i+1} - h_i) r(x_i, y_j, t) + (k_{j+1} - k_j) s(x_i, y_j, t),$$

where r, s depend on the derivatives of the entries of $\mathcal{A}$ of order less (or equal) to 2 and on the spatial derivatives of $p(t)$ of order less (or equal) to 3, and

$$|T^{(2)}_{\mathcal{L}_\mathcal{A}}(x_i, y_j, t)| \leq C H^2_{max} \|\mathcal{A}\|_{C^3_b(\mathbb{R}^2)} \|p(t)\|_{C^4(\overline{\Omega})}, \tag{34}$$

being C a positive constant $p(t)$, $\mathcal{A}$, t and H independent.

For the truncation error $T_{\mathcal{L}_\mathcal{B}}(t)$ defined by

$$T_{\mathcal{L}_\mathcal{B}}(t) = \mathcal{L}_\mathcal{B}(R_H c(t)) - R_H \nabla.(\mathcal{B} \nabla c(t)),$$

we have a representation analogous to the one established for $T_{\mathcal{L}_\mathcal{A}}(t)$ with $\mathcal{A}$ replaced by $\mathcal{B}$ and $p(t)$ replaced by $c(t)$.

The truncation error T_{∇_c} given by

$$T_{\nabla_c} = \nabla_c.(R_H c(t) v(D_H R_H p(t))) - R_H \nabla.(c(t) v(\nabla p(t))),$$

admits the representation

$$T_{\nabla_c}(t) = \sum_{\ell=1}^{3} T_{\nabla_c}^{(\ell)}(t),$$

where

$$T_{\nabla_c}^{(1)}(x_i, y_j, t) = (h_{i+1} - h_i) r(x_i, y_j, t) + (k_{j+1} - k_j) s(x_i, y_j, t),$$

representing r and s functions that depend on $\dfrac{\partial^2}{\partial x^2}\big(c(t)v_1(\nabla p(t))\big)$ and $\dfrac{\partial^2}{\partial y^2}\big(c(t)v_2(\nabla p)\big)$,

$$T_{\nabla_c}^{(2)}(t) = D_{c,x}\sigma_{1,H}(t) + D_{c,y}\sigma_{2,H}(t),$$

with

$$\sigma_{\ell,H}(t) = R_H c(t)\big(v_\ell(D_H R_H p(t)) - R_H v_\ell(\nabla p(t))\big), \ell = 1, 2,$$

and

$$|T_{\nabla_c}^{(3)}(x_i, y_j, t)| \leq C H_{max}^2 \|c(t)v(\nabla p(t))\|_{[C^3(\overline{\Omega})]^2},$$

where C is a positive constant H, t, c, p and v independent.

It is clear that $T_p(t)$ and $T_{c,p}(t)$ are of first order with respect to the norm $\|.\|_\infty$. Consequently, it is expectable that $e_p(t)$ and $e_c(t)$ are at least of first order. In what follows we establish that both errors are indeed of second order with respect to the norm $\|.\|_{1,H}$ and considering the inequality (10) we establish second convergence order with respect to the norm $\|.\|_\infty$. To conclude such results, we prove in what follows several propositions that will be used in the main result of this section Theorem 4.4.

Proposition 4.1. *The truncation error $T_{\mathcal{L}_\mathcal{A}}(t)$ satisfies the following*

$$\begin{aligned}(T_{\mathcal{L}_\mathcal{A}}(t), v_H)_H \ &\leq C\|A\|^2_{C_b^3(\mathbb{R}^2)}\|p(t)\|^2_{C^4(\overline{\Omega})}\big(\frac{1}{16\varepsilon^2} + \frac{1}{2\eta^2}\big)H_{max}^4 \\ &\quad + \varepsilon^2\|\nabla_{H-} v_H\|^2_{H-} + 3\eta^2\|v_H\|^2_H,\end{aligned} \tag{35}$$

for $v_H \in W_{H,0}$. In (35), $\varepsilon, \eta \neq 0$ are arbitrary constant and C represents a constant H and t independent.

Proof: Using the definition of $T^{(1)}_{\mathcal{L}_\mathcal{A}}$ we have

$$\begin{aligned}(T^{(1)}_{\mathcal{L}_\mathcal{A}}(t), v_H)_H &= \sum_{i,j=1}^{N-1,M-1} h_{i+\frac{1}{2}} k_{j+\frac{1}{2}} (h_{i+1} - h_i) r(x_i, y_j, t) v_H(x_i, y_j) \\ &\quad + \sum_{i,j=1}^{N-1,M-1} h_{i+\frac{1}{2}} k_{j+\frac{1}{2}} (k_{j+1} - k_j) s(x_i, y_j, t) v_H(x_i, y_j).\end{aligned}$$

As $v_H(x_0, y_j) = v_H(x_N, y_j) = 0$, for the first term of the second member of the last equality we deduce, successively,

$$\begin{aligned}&\frac{1}{2} \sum_{i,j=1}^{N-1,M-1} k_{j+\frac{1}{2}} (h^2_{i+1} - h^2_i) r(x_i, y_j, t) v_H(x_i, y_j) \\ = \;& \frac{1}{2} \sum_{i,j=1}^{N,M-1} k_{j+\frac{1}{2}} h_i^2 \big(r(x_{i-1}, y_j, t) v_H(x_{i-1}, y_j) - r(x_i, y_j, t) v_H(x_i, y_j) \big) \\ = \;& -\frac{1}{2} \sum_{i,j=1}^{N,M-1} k_{j+\frac{1}{2}} h_i^3 r(x_{i-1}, y_j, t) D_{-x} v_H(x_i, y_j) \\ & -\frac{1}{2} \sum_{i,j=1}^{N,M-1} k_{j+\frac{1}{2}} h_i^2 \int_{x_{i-1}}^{x_i} \frac{\partial r}{\partial x}(x, y, t)\, dx v_H(x_i, y_j) \\ \leq \;& \frac{1}{2} \|r(t)\|_{C^0(\overline{\Omega})} H^2_{max} \sum_{i,j=1}^{N,M-1} k_{j+\frac{1}{2}} h_i |D_{-x} v_H(x_i, y_j)| \\ & + \frac{1}{2} \|r(t)\|_{C^1(\overline{\Omega})} H^2_{max} \sum_{i,j=1}^{N,M-1} k_{j+\frac{1}{2}} h_i |v_H(x_i, y_j)| \\ \leq \;& H^4_{max} \|r(t)\|^2_{C^1(\overline{\Omega})} \big(\frac{1}{16\varepsilon^2} + \frac{1}{4\eta^2} \big) + \varepsilon^2 \|D_{-x} v_H\|^2_{h-} + \eta^2 \|v_H\|^2_H),\end{aligned}$$

where $\varepsilon, \eta \neq 0$ are arbitrary constants.

As for the second term of $(T^{(1)}_{\mathcal{L}_\mathcal{A}}(t), v_H)_H$ admits the upper bound

$$\sum_{i,j=1}^{N-1,M-1} h_{i+\frac{1}{2}} k_{j+\frac{1}{2}} (k_{j+1} - k_j) s(x_i, y_j, t) v_H(x_i, y_j)$$
$$\leq H^4_{max} \|s(t)\|^2_{C^1(\overline{\Omega})} \big(\frac{1}{16\varepsilon^2} + \frac{1}{4\eta^2}\big) + \varepsilon^2 \|D_{-y} v_H\|^2_{k-} + \eta^2 \|v_H\|^2_H,$$

we obtain

$$\begin{aligned}(T^{(1)}_{\mathcal{L}_\mathcal{A}}(t), v_H)_H \leq H^4_{max} \big(\|r(t)\|^2_{C^1(\overline{\Omega})} + \|s(t)\|^2_{C^1(\overline{\Omega})}\big) \big(\tfrac{1}{16\varepsilon^2} + \tfrac{1}{4\eta^2}\big) \\ + \varepsilon^2 \|\nabla_{H-} v_H\|^2_{H-} + 2\eta^2 \|v_H\|^2_H.\end{aligned} \tag{36}$$

From (34), taking into account that

$$\begin{aligned}(T^{(2)}_{\mathcal{L}_\mathcal{A}}(t), v_H)_H &\leq \frac{1}{4\eta^2} \|T^{(2)}_{\mathcal{L}_\mathcal{A}}(t)\|^2_H + \eta^2 \|v_H\|^2_H \\ &\leq C H^4_{max} \|\mathcal{A}\|^2_{C^3_b(\mathbb{R}^2)} \|p(t)\|_{C^4(\overline{\Omega})} + \eta^2 \|v_H\|^2_H,\end{aligned} \tag{37}$$

we conclude (35).

■

Proposition 4.2. *For the truncation error $T_{\mathcal{L}_\mathcal{B}}(t)$ we have*

$$\begin{aligned}(T_{\mathcal{L}_\mathcal{B}}(t), v_H)_H \leq\ & C \|B\|^2_{C^3_b(\mathbb{R})} \|c(t)\|^2_{C^4(\overline{\Omega})} \big(\frac{1}{16\varepsilon^2} + \frac{1}{2\eta^2}\big) H^4_{max} \\ & + \varepsilon^2 \|\nabla_{H-} v_H\|^2_{H-} + 3\eta^2 \|v_H\|^2_H,\end{aligned} \tag{38}$$

for $v_H \in W_{H,0}$. In (38), $\varepsilon, \eta \neq 0$ are arbitrary constant and C represents a constant H and t independent.

We observe that, if $v_H \in W_{H,0}$, then for $(T^{(1)}_{\nabla_c}(t), v_H)_H$ and $(T^{(3)}_{\nabla_c}, v_H)_H$ hold estimates analogous to (36) and (37), respectively. To conclude an estimate for $(T_{\nabla_c}(t), v_H)_H$ we need to establish an upper bound for $(T^{(2)}_{\nabla_c}(t), v_H)_H$. As v_H and $\sigma_{\ell,H}$ are null on $\partial\Omega_H$, it can be shown that

$$\begin{aligned}(D_{c,x} \sigma_{1,H}(t), v_H)_H = \frac{1}{2} \sum_{i,j=1}^{N,M-1} k_{j+\frac{1}{2}} \sigma_{1,H}(x_i, y_j, t) \Big(h_{i+1} D_{-x} v_H(x_{i+1}, y_j) \\ + h_i D_{-x} v_H(x_i, y_j) \Big).\end{aligned}$$

Using the fact that D_H is a second order operator also in not uniform meshes

$$|\sigma_{1,H}(x_i, y_j, t)| \leq L_v \|c(t)\|_{C^0(\overline{\Omega})} \|p(t)\|_{C^3(\overline{\Omega})} H^2_{max},$$

we get

$$(D_{c,x}\sigma_{1,H}(t), v_H)_H \leq \frac{1}{4\varepsilon^2} L_v^2 \|c(t)\|^2_{C^0(\overline{\Omega})} \|p(t)\|^2_{C^3(\overline{\Omega})} H^4_{max} + \varepsilon^2 \|D_{-x} v_H\|^2_{h-},$$

where $\varepsilon \neq 0$ is an arbitrary constant.

Following for $(D_{c,y}\sigma_{2,H}(t), v_H)_H$ the procedure used to get the upper bound for $(D_{c,x}\sigma_{1,H}(t), v_H)_H$, we conclude that

$$(T^{(2)}_{\nabla_c}(t), v_H)_H \leq \frac{1}{2\varepsilon^2} L_v^2 \|c(t)\|^2_{C^0(\overline{\Omega})} \|p(t)\|^2_{C^3(\overline{\Omega})} H^4_{max} + \varepsilon^2 \|\nabla_{H-} v_H\|^2_{H-}.$$

We proved the next proposition.

Proposition 4.3. *If $c(t) \in C^3(\overline{\Omega}), p \in C^4(\overline{\Omega}), v \in [C^3_b(\mathbb{R})]^2$, then, for $v_H \in W_{H,0}$, we have*

$$\begin{aligned}(T_{\nabla_c}(t), v_H)_H \leq\ & C\|v\|^2_{[C^3_b(\mathbb{R})]^2} \|c(t)\|^2_{C^3(\overline{\Omega})} \|p(t)\|^2_{C^4(\overline{\Omega})} \big(\frac{9}{16\varepsilon^2} + \frac{1}{2\eta^2}\big) H^4_{max} \\ & + 2\varepsilon^2 \|\nabla_{H-} v_H\|^2_{H-} + 3\eta^2 \|v_H\|^2_H,\end{aligned} \tag{39}$$

where $\varepsilon, \eta \neq 0$, C denotes a positive constant H and t independent.

We are now ready to prove the main result of this section:

Theorem 4.4. *Let us suppose that the solution of the differential-algebraic IBVP (1) c and p is such that $c \in C^1([0,T], C^0(\overline{\Omega})) \cap L^\infty([0,T], C^4(\overline{\Omega}))$, $p \in L^\infty([0,T], C^4(\overline{\Omega}))$, and the solution of the c_H, p_H of the differential algebraic IVP (11) is such that $c_H \in C^1([0,T], W_{H,0}))$ and $p_H(t) \in W_{H,0}, t \in (0,T]$ and let $e_c(t) = R_H c(t) - c_H(t), e_p(t) = R_H p(t) - p_H(t)$ be the correspondent spatial discretization errors. If the sequnce of spatial grids $\overline{\Omega}_H, H \in \Lambda$, satisfies (25), for H_{max} small enough, and $a_H(.,.), b_H(.,.)$ are elliptic in $[W_{H,0}]^2$ with ellipticity constants $C_{e,a}$ and $C_{e,b}$ H independent, then, for H_{max} small enough, there exists a positive constant C that is H, t, c and p independent, such that*

$$\begin{aligned}&\|e_c(t)\|^2_H + C_{e,b} \int_0^t e^{\int_s^t g_H(c(\mu))d\mu} \|e_c(s)\|^2_{1,H} ds \\ &\quad \leq C H^4_{max} \int_0^t e^{\int_s^t g_H(c(\mu))d\mu} \Big((\|c(s)\|^2_\infty + \|c(s)\|^2_{C^3(\overline{\Omega})}) \|p(s)\|^2_{C^4(\overline{\Omega})} \\ &\qquad\qquad + \|c(s)\|^2_{C^4(\overline{\Omega})} \Big) ds,\end{aligned} \tag{40}$$

$$\|e_p(t)\|^2_{1,H} \leq CH^4_{max}\Big(\frac{\|\alpha\|^2_\infty}{2C^2_{e,a}}\int_0^t e^{\int_s^t g_H(c(\mu))d\mu}\Big((\|c(s)\|^2_\infty + \|c(s)\|^2_{C^3(\overline{\Omega})})\|p(s)\|^2_{C^4(\overline{\Omega})} + \|c(s)\|^2_{C^4(\overline{\Omega})}\Big)ds + \|p(t)\|^2_{C^4(\overline{\Omega})}\Big), \tag{41}$$

for $t \in [0,T]$. *In (41),* $g_H(c(t))$ *is defined by*

$$g_H(c(t)) = \frac{13}{C_{e,b}}\big(2\frac{\|\alpha\|^2_\infty}{C^2_{e,a}}L^2_v C^2_g\|c(t)\|^2_\infty + \|v\|^2_\infty\big) + 2\|\beta\|_\infty. \tag{42}$$

Proof: From (33), we easily get

$$C_{e,a}\|e_p(t)\|^2_{1,H} \leq \frac{1}{4\eta^2}\|\alpha\|^2_\infty\|e_c(t)\|^2_H + \eta^2\|e_p(t)\|^2_H + (T_p(t), e_p(t))_H, \tag{43}$$

where $\eta \neq 0$ is an arbitrary constant, and

$$\begin{aligned}\frac{1}{2}\frac{d}{dt}\|e_c(t)\|^2_H \;&+C_{e,b}\|e_c(t)\|^2_{1,H} \leq \|\beta\|_\infty\|e_c(t)\|^2_H + (T_{c,p}(t), e_c(t))_H \\ &+(M_H(R_Hc(t)v(D_H(R_Hp(t))) - c_H(t)v(D_H(p_H(t)))), \nabla_{H-}e_c(t))_{H-}.\end{aligned} \tag{44}$$

Taking into account Proposition 4.1, from (43), we obtain

$$\begin{aligned}\big(C_{e,a} - 4\eta^2)\|e_p(t)\|^2_H + \big(C_{e,a} - \varepsilon^2\big)\|\nabla_{H-}e_p(t)\|^2_{H-} \leq \frac{\|\alpha\|^2_\infty}{4\eta^2}\|e_c(t)\|^2_H \\ +CH^4_{max}\|\mathcal{A}\|^2_{C^3_1(\mathbb{R}^2)}\|p(t)\|^2_{C^4(\overline{\Omega})},\end{aligned} \tag{45}$$

where C depends on $\eta^{-2}, \varepsilon^{-2}$. Fixing conveniently η and ε in (45), we deduce

$$\|e_p(t)\|^2_{1,H} \leq \frac{\|\alpha\|^2_\infty}{2C^2_{e,a}}\|e_c(t)\|^2_H + CH^4_{max}\|\mathcal{A}\|^2_{C^3_b(\mathbb{R}^2)}\|p(t)\|^2_{C^4(\overline{\Omega})}. \tag{46}$$

As done in (30), we have

$$\begin{aligned}(M_H\big(R_Hc(t)v(D_HR_Hp(t)) - c_H(t)v(D_Hp_H(t))\big), \nabla_{H-}e_c(t))_{H-} \\ \leq \frac{2}{\eta^2}L^2_vC^2_g\|R_Hc(t)\|^2_\infty\|\nabla_{H-}e_p(t)\|^2_{H-} + \frac{1}{2\eta^2}\|v\|^2_\infty\|e_c(t)\|^2_H \\ +2\eta^2\|\nabla_{H-}e_c(t)\|^2_{H-},\end{aligned}$$

where $\eta \neq 0$ is an arbitrary constant. Taking now into account (46), we obtain

$$\begin{aligned}(M_H\big(R_H c(t)v(D_H R_H p(t)) - c_H(t)v(D_H p_H(t))\big), \nabla_{H-} e_c(t))_{H-} \\ \leq \big(\frac{1}{\eta^2} L_v^2 C_g^2 \frac{\|\alpha\|_\infty^2}{C_{e,a}} \|c(t)\|_\infty^2 + \frac{1}{2\eta^2}\|v\|_\infty^2\big)\|e_c(t)\|_H^2 + 2\eta^2 \|\nabla_{H-} e_c(t)\|_{H-}^2 \\ + C H_{max}^4 \frac{L_v^2 C_g^2}{\eta^2} \|\mathcal{A}\|_{C_b^3(\mathbb{R}^2)}^2 \|p(t)\|_{C^4(\overline{\Omega})}^2 \|c(t)\|_\infty^2.\end{aligned}$$

Inserting the last upper bound in (44), considering Propositions 4.2 and 4.3 and choosing conveniently η^2 and ε^2, it can be shown that holds the following differential inequality

$$\frac{d}{dt}\|e_c(t)\|_H^2 + C_{e,b}\|e_c(t)\|_{1,H}^2 \leq g_H(c(t))\|e_c(t)\|_H^2 + T_H(t), \tag{47}$$

with $g_H(c(t))$ defined by (42) and $T_H(t)$ given by

$$T_H(t) = C H_{max}^4 \Big((\|c(t)\|_\infty^2 + \|c(t)\|_{C^3(\overline{\Omega})}^2)\|p(t)\|_{C^4(\overline{\Omega})}^2 + \|c(t)\|_{C^4(\overline{\Omega})}^2 \Big),$$

and C is a positive constant H,t, c and p independent.

The differential inequality (47) leads to (40). Finally, combining (40) with (46) we conclude (41).

■

5. Numerical simulation - convergence results

This section aims to illustrate the main convergence result of this paper: Theorem 4.4, more precisely the error estimates (40) for the concentration error $e_c(t) = R_H c(t) - c_H(t)$ and (41) for the pressure error $e_p(t) = R_H p(t) - p_H(t)$, where $p_h(t)$ and $c_H(t)$ are defined by the differential algebraic problem (11).

In the time interval $[0, T]$ we fix the time grid $\{t_n, n = 0, \ldots, M\}$ with fixed time step $\Delta_t = T/M$ and the time integration of the initial value differential-algebraic problem (11) using the implicit-explicit method

$$\begin{cases} -\mathcal{L}_{\mathcal{A}} p_H^{n+1} = R_H \alpha c_H^n, \\ \dfrac{c_h^{n+1} - c_H^n}{\Delta_t} + \nabla_c \cdot (c_H^n v(D_H p_H^{n+1})) = \mathcal{L}_{\mathcal{B}}(c_H^{n+1}) + R_H \beta c_H^n, \\ \qquad\qquad\qquad\qquad\qquad\qquad \text{in } \Omega_H, n = 0, \ldots, M-1, \\ p_H^n = c_H^n = 0, \ \text{ on } \partial\Omega_H, n = 1, \ldots, M, \\ c_H^0 = R_H c_0, \ \text{ in } \Omega_H. \end{cases} \tag{48}$$

In what follows we consider the following notations

$$\|e_p\|_H = \max_{n=1,\dots,M} \|e_p^n\|_H, \tag{49}$$

where $e_p^n = R_H p(t_n) - p_H^n$, and

$$\|e_c\|_H = \max_{n=1,\dots,M} \sqrt{\|e_H^n\|_H^2 + \sum_{j=1}^{n} \Delta_t \|\nabla_{H-} e_H^j\|_{H-}^2}, \tag{50}$$

with $e_c^j = R_H c(t_j) - c_H^j$. We also consider

$$Rate_i = \frac{\log \dfrac{\|e_i\|_H}{\|e_i\|_{\tilde{H}}}}{\log \dfrac{H_{max}}{\tilde{H}_{max}}}, \tag{51}$$

for $i = p, c$.

Example 5.1. *We start by considering a regular C^4 solution*

$$p(x, y, t) = c(x, y, t) = e^{-t} \sin(\pi x) \sin(\pi y),$$

defined in $[0, 1]^2 \times [0, T]$, with $T = 0.1$, $\Delta_t = 10^{-3}$,

$$\mathcal{A}(x, y) = \begin{bmatrix} 4 + \sin(\pi y)^2 & -\sin(\pi x) \sin(\pi y) \\ -\sin(\pi x) \sin(\pi y) & 4 + \sin(\pi x)^2 \end{bmatrix}, D = \frac{1}{8\pi^2},$$

The errors $\|e_p\|_H$ $\|e_c\|_H$ for the numerical approximations defined by 48 as well as the convergence rates are included in Table 1 and in Figures 3(a) and 3(b).

TABLE 1. Numerical errors and convergence rates in Example 5.1

H_{max}	$\|e_p\|_H$	Rate$_p$	$\|e_C\|_H$	Rate$_C$
2.503216e-01	1.706188e-01	-	3.505003e-01	-
1.252408e-01	3.605839e-02	2.244438	7.620294e-02	2.203528
8.342393e-02	1.541813e-02	2.091040	3.357726e-02	2.017093
6.255882e-02	8.574553e-03	2.038528	1.906057e-02	1.967243
5.023403e-02	5.469237e-03	2.049362	1.224774e-02	2.015729
4.204243e-02	3.793964e-03	2.054495	8.511195e-03	2.044562

FIGURE 1. Convergence rates in Example 5.1

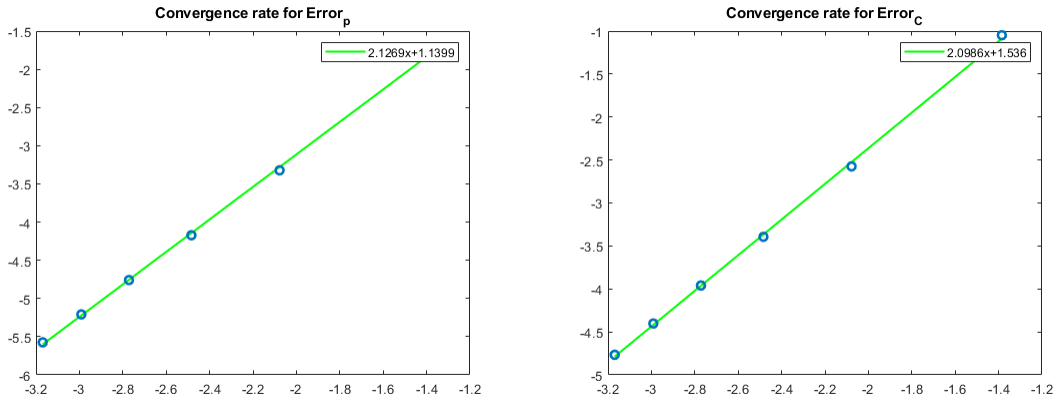

(a) $\|e_p\|_H$ (b) $\|e_C\|_H$

Example 5.2. *In what follows we reduce the smoothness of the solution of the differential problem under consideration. We take*

$$p(x,y,t) = \begin{cases} e^{8-t}((x-\frac{1}{10})(x-\frac{9}{10})(y-\frac{1}{10})(y-\frac{9}{10}))^4, \\ \qquad\qquad \frac{1}{10} \le x,y \le \frac{9}{10}, \\ 0, \textit{ otherwise}, \end{cases} \tag{52}$$

and (53)

$$c(x,y,t) = e^{-t}\sin(\pi x)\sin(\pi y). \tag{54}$$

with $\Omega = (0,1)^2$, $T = 0.1$, $\Delta_t = 10^{-3}$ *and*

$$\mathcal{A}(x,y) = \begin{bmatrix} 1+\sin(\pi y)^2 & -\sin(\pi x)\sin(\pi y) \\ -\sin(\pi x)\sin(\pi y) & 1+\sin(\pi x)^2 \end{bmatrix}, D = \frac{1}{2\pi^2}$$

Table 2 and Figures 3(a) and 3(b). Even with reduced smoothness, the numerical results also present second convergence rate.

TABLE 2. Numerical errors and convergence rates in Example 5.2

H_{max}	$\|e_p\|_H$	Rate$_p$	$\|e_C\|_H$	Rate$_C$
8.340501e-02	4.244955e-04	-	1.855296e-03	-
7.699766e-02	3.614419e-04	2.011679	1.590796e-03	1.924220
7.149196e-02	3.127291e-04	1.951262	1.381933e-03	1.897174
6.673173e-02	2.732260e-04	1.959786	1.209120e-03	1.938781
6.254805e-02	2.412143e-04	1.924663	1.069797e-03	1.890848
5.900608e-02	2.144615e-04	2.016581	9.522958e-04	1.995874
5.560734e-02	1.909160e-04	1.960324	8.492288e-04	1.930827
5.280920e-02	1.713778e-04	2.091092	7.651417e-04	2.019521

FIGURE 2. Convergence rates in Example 5.2

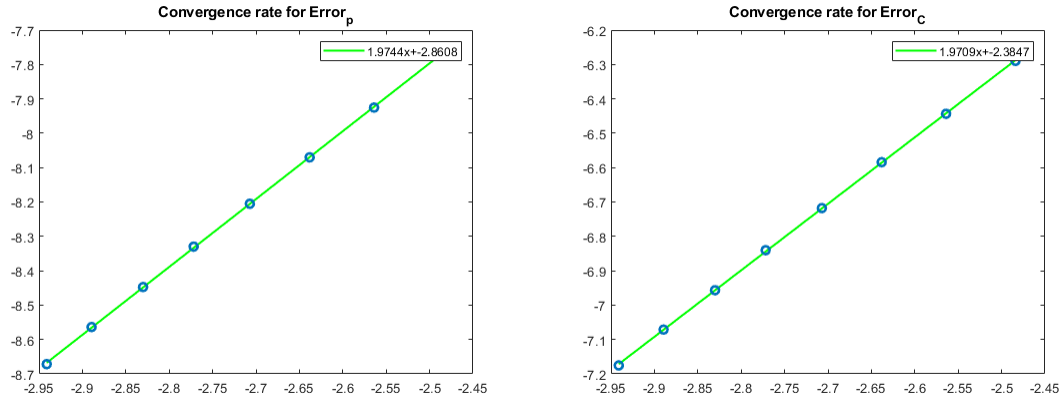

(a) $\|e_p\|_H$ (b) $\|e_C\|_H$

6. Modeling the cell dynamics in a colonic crypt by a elliptic-parabolic PDE system

A crypt Γ in the colon epithelium has a geometry similar to that shown in figure (3) (see [10, 13, 12]).

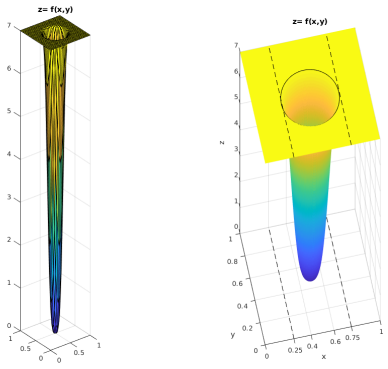

FIGURE 3. Different views of the epithelium crypt geometry Γ defined by the graph of $z = f(x, y)$ given in (55)-(56).

On averaging, a crypt has a height that is almost 14 times the diameter of the top crypt orifice, in particular, its height from the bottom to the top orifice is $433\mu m$ and the diameter of the top orifice is $31.1\mu m$ including the epithelium tissue ([10]). After a proper scaling of their dimensions we get for a standard crypt Γ a height $h = 7\mu m$ and a radius $R = 0.25\mu m$, and we assume that a crypt can be seen as a two dimensional manifold Γ represented by the the graph of a continuum and differentiable function $f : \overline{\Omega} \to \mathbb{R}$

$$\Gamma = \{(x, y, z) \in \mathbb{R}^3 : (x, y) \in \overline{\Omega}, z = f(x, y)\}, \tag{55}$$

where $\overline{\Omega} = [0, 1]^2$ and f is the following function

$$f(x, y) = h(1 - e^{-\left(\frac{R(x,y)}{\sigma}\right)^2}), \quad (x, y) \in \overline{\Omega}, \tag{56}$$

with $R(x, y) = (x - 1/2)^2 + (y - 1/2)^2$, and $\sigma > 0$. In the following we use $\sigma = 0.03\mu_m$ that allows to have a crypt with height $h = 7\mu m$ and a top crypt radius $R = 0.25\mu m$, see Figure 3.

Inside a normal epithelium crypt, stem cells live and are fixed at the crypt bottom. Their differentiation give rise to semi-differentiated cells (also called transit cells) that can migrate upwards in the direction of the top orifice. During this migration, transit cells continue to differentiate and become fully differentiated (or mature) at the crypt top [18, 17, 19]. Cell location of these three families of cells are depicted in Figure 6.

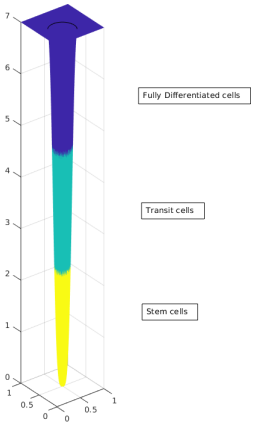

FIGURE 4. Stem, transit and fully-differentiated cells location in a normal crypt.

In order to model the cell dynamics in a crypt, we denote by $c(x, y, z, t)$ the density of the stem and semi–differentiated cells located at $(x, y, z) \in \Gamma$ at time t. The semi–differentiated cells are under the effect of a cell-cell adhesion pressure $p(x, y, z, t)$, at $(x, y, z) \in \Gamma$ at time t, that is responsible for the cell migration. Then considering the mathematical models in [11, 12, 13] for the colon cell dynamics, the behavior of the colonic cell density c and pressure p can be described by the following IBVP

$$\begin{cases} -\xi \Delta_\Gamma p = \alpha c, \\ \dfrac{\partial c}{\partial t} - \nabla_\Gamma \cdot (\xi c \nabla_\Gamma p) = \nabla_\Gamma \cdot (D \nabla_\Gamma c) + \beta c, \ \text{ in } \Gamma \times (0, T], \\ p = c = 0, \quad \text{ on } \partial\Gamma \times (0, T], \\ c(0) = c_0, \quad \text{ in } \Gamma, \end{cases} \tag{57}$$

where the diffusion coefficient D is supposed constant, and ξ is a positive constant that depends on the permeability and viscosity of the epithelium tissue [11]. The cell velocity v in (57) is given in fact by Darcy's law $v(\nabla_\Gamma p) = -\xi \nabla_\Gamma p$, as it will be analyzed later. Here the operators ∇_Γ and Δ_Γ are the gradient and Laplace operators acting on the spatial variables x, y, z on the crypt manifold Γ. In (57), the function c_0 describes the initial distribution of cell density in the crypt, α is the proliferation rate for the stem and transit cells, and β is defined by $\beta = \alpha - \gamma$, where γ denotes the rate of transformation of the transit cells into fully differentiated cells. In a normal epithelium crypt, γ is considered null at the crypt bottom where no transit

cells are present and increases along the crypt axis up to two thirds of its height where thereafter only mature cells reside [22, 20].

Since in the normal epithelium cell behavior in the crypt is basically invariant in time depending only on their relative position with respect the crypt bottom ([18, 17, 19]), the functions α, β, γ can be assumed constant in time depending only on the cell quote z along the vertical crypt axis. Then we consider $\alpha(x,y,z,t) = \alpha(z)$, $\beta(x,y,z,t) = \beta(z)$ and $\gamma(x,y,z,t) = \gamma(z)$, for all $(x,y,z) \in \Gamma$. Thus, in normal epithelium, we can assume that we have a stable cell density of type $c(x,y,z,t) = c_{stab}(z)$ and also the pressure p satisfies $p(x,y,z,t) = p_{stab}(z)$ for all $(x,y,z) \in \Gamma$.

In [11, 12, 13], a PDE model similar to (57) has been studied considering only the transit cell density. In order to define a more precise and complete model, here c represents the density of the stem and transit cells, where the latter differs from the first for its location in the middle of the crypt axis. Moreover, transit cells have larger proliferation, they move in the transition phase whereas stem cells are fixed and proliferate very slowly.

We remark that the PDE model (57) can be used to describe the colon cell dynamics in a normal epithelium crypt, as well as in an abnormal crypt, by changing the parameters, the initial condition c_0 and the rate functions α, β, as it will be discussed later.

We start now to specify the parameters and rate functions in (57) to describe the cell dynamics in a normal crypt. It has been observed that the proliferation rate α is very low at the crypt bottom where stem cells are located and rapidly increases along the crypt axis up to reach almost one third of the crypt height [21, 22]. Then it decreases up to reach a quote $\frac{2}{3}h$ so that transit cells proliferate up to two-thirds of the crypt height [17, 20]. Based on this biological information, we use the following expression for the proliferation rate in a normal epithelium crypt of height h

$$\alpha(z) = \begin{cases} \tau \left(1 - \dfrac{z}{\frac{1}{3}h}\right)^2 \left(1 - \dfrac{z}{\frac{2}{3}h}\right)^2 e^{-(z-\frac{h}{3})^2}, & \dfrac{h}{3} \leq z \leq \dfrac{2}{3}h, \\ 0, \quad \dfrac{2}{3}h < z \leq h \text{ or } 0 \leq z < \dfrac{h}{3}, \end{cases} \tag{58}$$

where $\tau > 0$ is a constant that will be estimated later. A plot for the rate α defined by (58) is presented in Figure 5.

Note that α depends only on the relative position of z with respect the crypt height h, and it is null in the crypt bottom below the quote $z = \frac{h}{3}$.

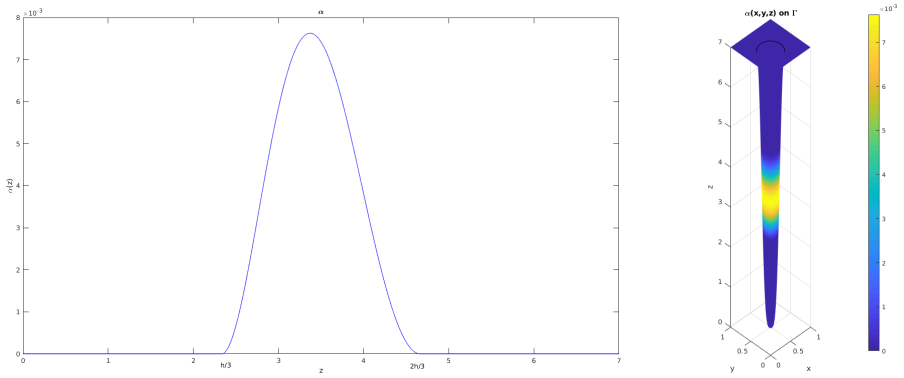

FIGURE 5. Proliferation rate α of stem and transit cells in a normal epithelium crypt along its vertical axis (left figure) and on the crypt manifold Γ (right figure) for $h = 7$, $\sigma = 0.03$ and $\tau = 0.60974$.

This assumption reflects the fact that the stem cells that are filling the crypt base are not proliferating in short time periods, as evidenced in [21, 22], and permits to have a null velocity at the crypt bottom, as it is expected, since stem cells located there are fixed.

To have a natural and phenomenological construction of the function γ, we introduce a time independent solution c_{stab} of (57) that is able to capture some biological information: in the normal epithelium only stem cells are locates in the crypt bottom and no transit cells or stem cells are found in the last third of the crypt height. As in [11, 13], in the region where $c = 1$ no fully differentiated cells are found and, viceversa, where $c = 0$ then only fully differentiated cells are present. As normal cell density for the stem and semi-differentiated cells we consider

$$c_{stab}(z) = \begin{cases} \tau\left(\frac{2}{3}h - z\right) r(z) e^{-(z-\frac{h}{3})^2}, & \frac{h}{3} \le z \le \frac{2}{3}h, \\ 1, \quad 0 \le z \le \frac{h}{3}, \\ 0, \quad \frac{2}{3}h < z \le h, \end{cases} \tag{59}$$

with $r(z) = -\frac{54}{h^3}z^2 + \frac{45}{h^2}z - \frac{6}{h}$ that guarantees that $c'_{stab}(\frac{h}{3}) = c'_{stab}(\frac{2}{3}h) = 0$, and that $0 \le c_{stab} \le 1$.

In Figure 6 we plot c_{stab} in the crypt Γ with height $h = 7$ and $\sigma = 0.03$ (left) and its contour plot (right).

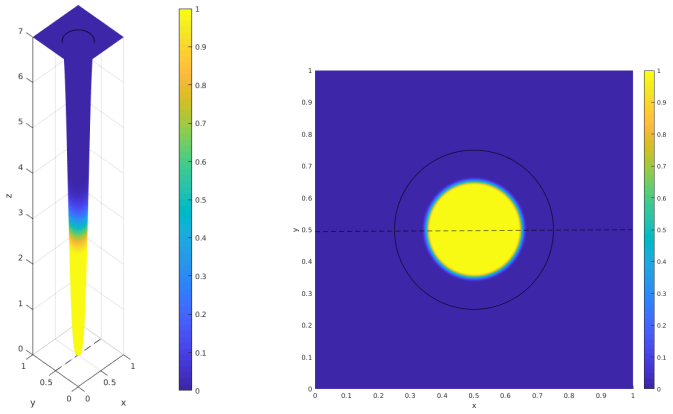

FIGURE 6. Left: Plot of c_{stab} in the crypt manifold Γ. Right: Contour plot of $c_{stab}(f(x,y))$ for $(x,y) \in \overline{\Omega}$.

The function γ is now computed considering that c_{stab} is an invariant stable solution of the PDE system (57). In fact, from (57) and taking into account that $\beta = \alpha - \gamma$, we obtain the transformation rate γ of transit cells into fully differentiated cells for $z \in (\frac{h}{3}, \frac{2h}{3})$

$$\gamma = \frac{1}{c_{stab}}\big(\nabla_\Gamma(\xi c_{stab}\nabla_\Gamma p_{stab}) + \nabla(D\nabla c_{stab})\big) + \alpha, \tag{60}$$

where p_{stab} is such that $-\xi\Delta_\Gamma p_{stab} = \alpha c_{stab}$ holds in Γ and $p_{stab} = 0$ on $\partial\Gamma$. Note that since α and c_{stab} are invariant with respect x, y and depends only on z, for $(x,y,z) \in \Gamma$, then also the transformation rate γ given in (60) depends only on z. In Figure 6 we illustrate the behaviour of γ for $D = 10^{-05}$, $\tau = 0.60974$ and $\xi = 0.02473$.

Since no cell transformation is active where there are no transit cells, as we have for $z \leq \frac{h}{3}$ or $z \geq \frac{2h}{3}$, thus we take $\gamma(z) = 0$ for $z \leq \frac{h}{3}$ or $z \geq \frac{2h}{3}$.

Consequently, β in the normal epithelium crypt is given by $\beta(z) = \alpha(z) - \gamma(z)$ with

$$\beta(z) = \begin{cases} \tau\left(1 - \dfrac{z}{\frac{1}{3}h}\right)^2\left(1 - \dfrac{z}{\frac{2}{3}h}\right)^2 e^{-(z-\frac{h}{3})^2} - \gamma(z), & \dfrac{h}{3} < z < \dfrac{2}{3}h, \\ 0, \, 0 \leq z \leq \dfrac{h}{3} \text{ or } \dfrac{2}{3}h \leq z \leq h. \end{cases} \tag{61}$$

In order to complete system (57) to describe the cell dynamics in a normal epithelium crypt, we need to specify the positive constants τ and ξ. Note that these parameters appear in the first equation of system (57) in the left and right hand sides respectively. Then its ratio will depend on the

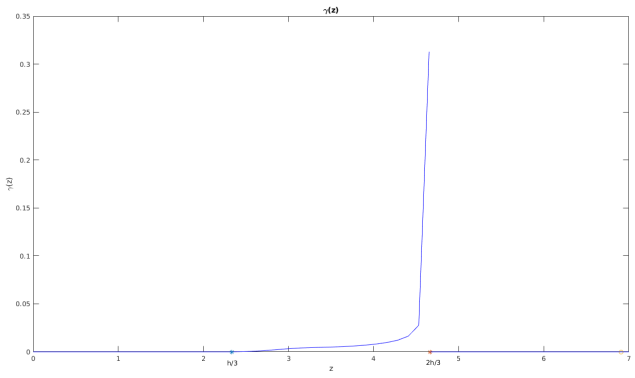

FIGURE 7. Transformation rate for semi-differentiated cells into fully differentiated cells in the normal epithelium with cell density $c_{stab}(z)$ and proliferation rate $\alpha(z)$.

pressure p_{stab} and cell density c_{stab} solution of (57) in normal epithelium and it will be deduced by using the known velocity of cells at the crypt top. In fact, it is known, see [17], that transit cells moves upwards along the vertical crypt height up to reach the crypt top with an increasing velocity that reaches an estimated maximum of 0.85 cell-position per hour at the crypt top. Since a cell-position along the crypt axis corresponds to the cell height, that is $5.9\mu m$, as estimated in [10] and in the references therein, then the maximum cell velocity is $0.85 \times 5.9\frac{\mu m}{hour}$. Since the height of a real crypt is $433\mu m$ (estimated value), the height of a single cell in a crypt with height h is obtained through a linear projection $h_{cell} = 5.9\frac{h}{433}$. For instance, for a crypt with height $h = 7\mu m$, the maximum velocity is then $v_{max} = 0.85 h_{cell} \approx 0.0811$. Note that since the first equation in (57) can be write as $\nabla \cdot \mathbf{v} = \alpha c$, with $\mathbf{v}(\nabla p) = -\xi \nabla p$, we can use the facts that α in (58) depends only on the crypt quote z and that it is null in the last third of the crypt height (for $z \geq \frac{2}{3}h$) to assert that the maximum velocity v_{max} is reached at the crypt quote $z = \frac{2h}{3}$ (see Figure 8).

In what follows we consider the abnormal case characterized by the formation of adenomas in the middle of the crypt axis due to an accumulation of transit proliferating cells that are hyper proliferating and are not able to complete their differentiation before the two thirds of the crypt height. This pathologic behaviour occurs due to the APC cell mutations occurring in the migrating transit cells. This early genetic hit can stop the differentiation process and perturbs the upward migration of the cells that it is so retained

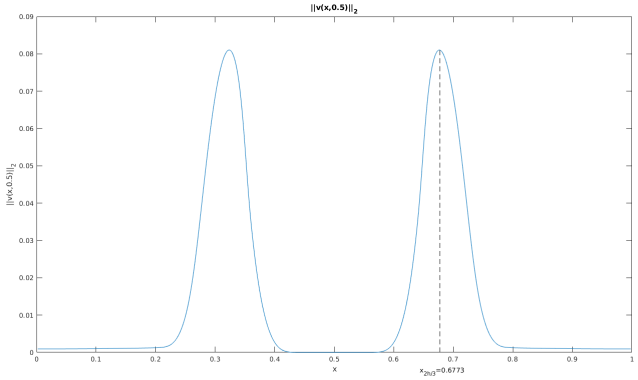

FIGURE 8. Plot of the euclidean norm of the cell velocity $\|v(x, 0.5, z)\|_2$, with $y = 0.5$, $z = f(x, 0.5)$ and $x \in (0, 1)$. The dashed line corresponds to $x = 0.6773$ that is where the Γ crypt quote $z = f(x, 0.5)$ is equal to $\frac{2}{3}h$.

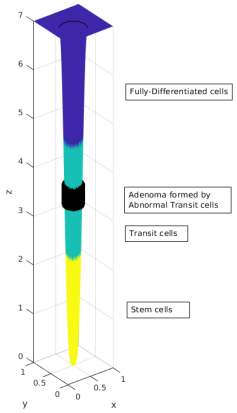

FIGURE 9. Abnormal transit cells forming an adenoma in the middle of the crypt marked in dark. This adenoma is in the transit region marked in light-blue.

in the middle of the colonic crypt. A such abnormal case was considered previously for instance in [23, 24]. A representation of what can happen it is represented in Figure 9.

In an abnormal epithelium crypt context, some of the biological facts examined before are not observed, in particular we are not able to assure a time stable solution c_{stab} along the time period of cell dynamics examined. This fact is consequence of the perturbation of the proliferation rate and the differentiation due to some cell mutations in the regular cell life cycle observed in normal crypts.

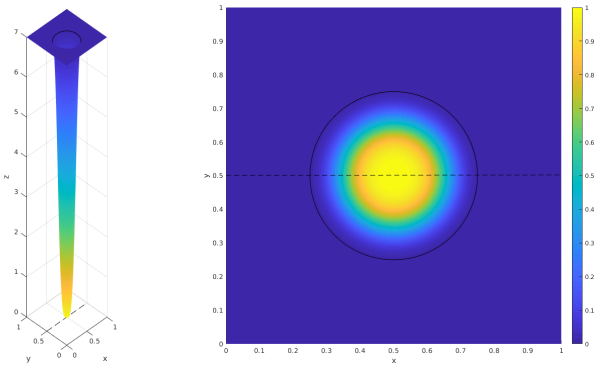

FIGURE 10. Left: Plot of $\tilde{c}_0$ defined in (62) in the crypt Γ. Right: Contour plot of $\tilde{c}_0(f(x,y))$ for $(x,y) \in \overline{\Omega}$.

To apply (57) in the description of the behaviour of abnormal cell proliferation and differentiation characterized by a growing adenoma, we need to change the parameters considered before in the normal case. For instance we should consider a higher proliferation rate with a coefficient τ that is 10 times higher than the one estimated in the normal epithelium, more precisely, we use $\tau = 0.60974 \cdot 10 = 6.0974$. In what concerns the differentiation process, it should stop in the transient region. This fact is achieved taking $\gamma(z) = 0$, for $z \in [\frac{h}{3}, \frac{2h}{3}]$. In what concerns the initial condition c_0 in the abnormal scenario we use $c(x,y,z,0) = c_0(x,y,z) = c_0(x,y,f(x,y)) = \tilde{c}_0(x,y)$ with

$$\tilde{c}_0(x,y) = \frac{xy(x-1)(y-1)}{(0.5)^4}\, e^{-\left(\frac{R(x,y)}{\sigma}\right)^2}, \quad (x,y) \in \overline{\Omega}. \tag{62}$$

Figure 10 illustrates the behaviour of $\tilde{c}_0$.

The last choice for the initial condition allows to describe the cell dynamics in a abnormal epithelium crypt considering at the initial time a larger number of transit cells in the middle of the crypt that leads to an adenoma formation and its growing.

To present some numerical experiments illustrating the cell dynamics in the abnormal case described by (57) we need to rewrite this system in an equivalent form (1). This procedure allow us to use the implicit-explicit method (48) studied in this paper. We start by remarking that $\Delta_\Gamma p$, $\nabla_\Gamma \cdot (\xi c \nabla_\Gamma p)$ and $\nabla_\Gamma \cdot (D \nabla_\Gamma c)$ are defined in $\Gamma \times (0,T]$, where Γ is the manifold defined by (55) with f given by (56). Let $\varphi : \Omega \to \Gamma$ be defined by $\varphi(x,y) = (x,y,f(x,y)), (x,y) \in \Omega$. We observe that $\{\Omega, \phi\}$ is a chart of the manifold

Γ. Now to simplify the rewriting of the PDE model in Γ we consider $(x, y) = (u_1, u_2) \in \Omega$ and let $(.,.)$ be the Euclidean inner product and let $G = [G_{i,j}]$ be the following matrix $G_{i,j} = (\frac{\partial \phi}{\partial u_i}, \frac{\partial \phi}{\partial u_j})$, $i, j = 1, 2$,

$$G = \begin{bmatrix} 1 + (\frac{\partial f}{\partial x})^2 & \frac{\partial f}{\partial x}\frac{\partial f}{\partial y} \\ \frac{\partial f}{\partial x}\frac{\partial f}{\partial y} & 1 + (\frac{\partial f}{\partial y})^2 \end{bmatrix}.$$

We observe that since $det(G) = 1 + (\frac{\partial f}{\partial x})^2 + (\frac{\partial f}{\partial x})^2$, then G is nonsingular. Let $\hat{p}(x, y, t) = p(\phi(x, y), t)$, $\hat{c}(x, y, t) = c(\phi(x, y), t), (x, y) \in \Omega$. Following [14, 15, 16], it can be shown that $\hat{c}$ and $\hat{p}$ satisfy the PDE system in $\Omega \times (0, T]$

$$\begin{cases} -\nabla \cdot (\xi \mathcal{A} \nabla p) = \sqrt{det(G)}\alpha c, \\ \sqrt{det(G)}\dfrac{\partial c}{\partial t} - \nabla \cdot (\xi \mathcal{A} \nabla p c) = \nabla \cdot (D \mathcal{A} \nabla c) + \sqrt{det(G)}\beta c, \text{ in } \Omega \times (0, T], \\ c = p = 0 \text{ on } \partial\Omega \times (0, T], \\ c(0) = \tilde{c}_0 \text{ in } \Omega, \end{cases} \tag{63}$$

where the hat notation was omitted for simplification. In (63) the following terms are used:
$\mathcal{A} = \sqrt{det(G)}G^{-1}$ that is

$$\mathcal{A} = \frac{1}{\sqrt{det(G)}} \begin{bmatrix} 1 + \left(\dfrac{\partial f}{\partial y}\right)^2 & -\dfrac{\partial f}{\partial x}\dfrac{\partial f}{\partial y} \\ -\dfrac{\partial f}{\partial x}\dfrac{\partial f}{\partial y} & 1 + \left(\dfrac{\partial f}{\partial x}\right)^2 \end{bmatrix}, \tag{64}$$

α defined in (58) and $\beta = \alpha$.

We consider then the problem of abnormal cell dynamics in a colonic crypt described by the system (63) with initial condition for the cell density given in (62).

The numerical solution of (63) with $T = 1$, is obtained by applying the implicit-explicit method (48) that is now written in the following form

$$\begin{cases} -\xi\mathcal{L}_{\mathcal{A}}p_H^{n+1} = R_H(\sqrt{detG}\alpha)c_H^n, \\ R_H(\sqrt{detG}\dfrac{c_h^{n+1}-c_H^n}{\Delta_t} + \nabla_c\cdot(c_H^n\mathbf{v}(D_Hp_H^{n+1})) = \mathcal{L}_{\mathcal{B}}(c_H^{n+1}) \\ \qquad\qquad +R_H(\sqrt{detG}\beta)c_H^n, \ \text{ in } \Omega_H, n = 0,\ldots,M-1, \\ p_H^n = c_H^n = 0, \qquad \text{on } \partial\Omega_H, n = 1,\ldots,M, \\ c_H^0 = R_H\tilde{c}_0 \qquad \text{in } \Omega_H. \end{cases} \tag{65}$$

with $\mathbf{v}(D_Hp_H^{n+1}) = -\xi\mathcal{A}D_Hp_H^{n+1}$. The numerical experiments were obtained with $h_{max} = 0.0021$ and $\Delta t = 0.1$.

The IBVP (57) or (63) with the parameters and initial condition defined before intent to model the cell dynamics in a abnormal epithelium crypt characterized by an APC cell mutation that appears on the daughter transit cells that are hyper proliferative and persistent in the transit region. The behaviour of the simulation results presented in what follows agree with the one described in the literature [23, 17, 24] where it is reported that abnormal proliferative cells presenting an APC mutation in the transit region are responsible by an adenoma formation that starts to fill the rest of the crypt moving upwards along the crypt axis.

Figure 11 illustrates the behaviour of the cell density c defined by (65) at $t = 1$. We observe an increasing of the cell density in the region around the circle centered in $(0.5, 0.5)$ and radius 0.2 which is the zone of the adenoma formation by the abnormal transit cells. This fact is well illustrated in the plot of $c(x, 0.5, 1)$, $x \in [0, 1]$, included in the bottom of this figure.

Figures 12, 13 and 14 illustrate the behavior of cell density, the adhesion pressure and the velocity norm in the curve of the manifold Γ defined by the intersection of Γ with the vertical plane $y = 0.5$ that is parallel to the xoz plane. In Figure 12 we observe that cells proliferate abnormally in a restricted zone leading to a rapidly increasing of the transit cells density. We observe the abnormal cell proliferation occur in the transit region for $x < x_{2h/3}$, being $x_{2h/3}$ the abscissa of $z = \frac{2h}{3}$. Consequently, the growing of this cell density leads to an increasing of the pressure in all domain as it can be seen in Figure 13.

The increasing of the pressure leads to an increasing of cell velocity and, in particular, we have an enlargement of the transit region. The cells reach

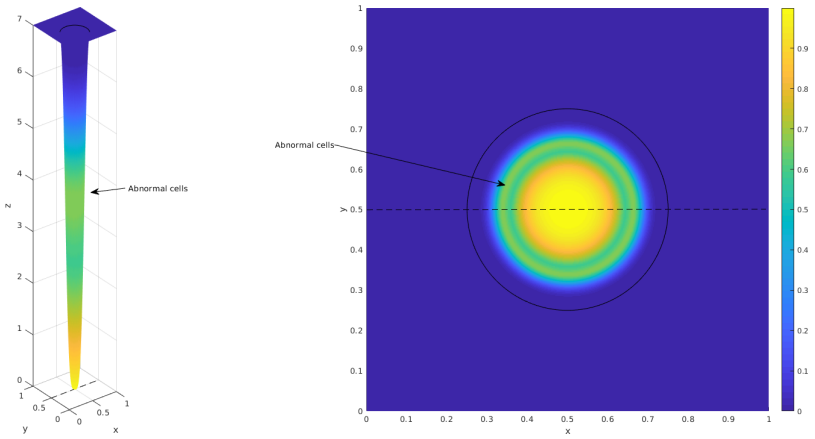

FIGURE 11. Left: Plot of the cell density c in the crypt Γ at time $t = 1$ with adenoma region. Right: Contour plot of the cell density $c(x, y, f(x, y), 1)$, $(x, y) \in \overline{\Omega}$, where the colored ring region is the location of the abnormal transit cells.

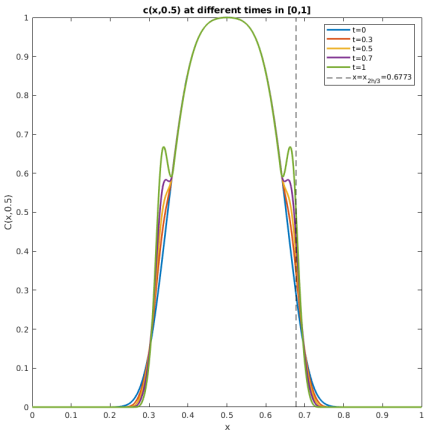

FIGURE 12. Plots of $c(x, 0.5, t)$ for $x \in [0, 1]$ and $t = 0, 0.3, 0.5, 0.7, 1$.

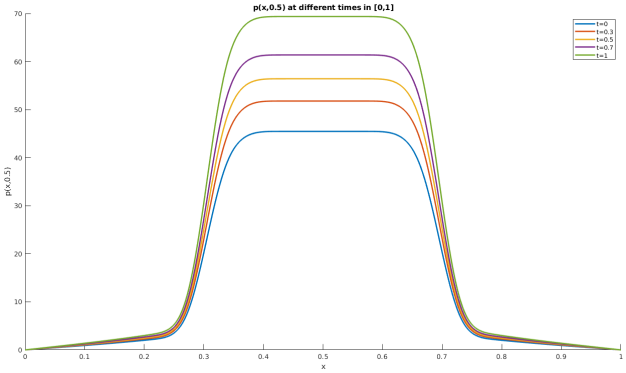

FIGURE 13. Pressure p at $y = 0.5$ and $x \in [0, 1]$ for $t = 0, 0.3, 0.5, 0.7, 1$.

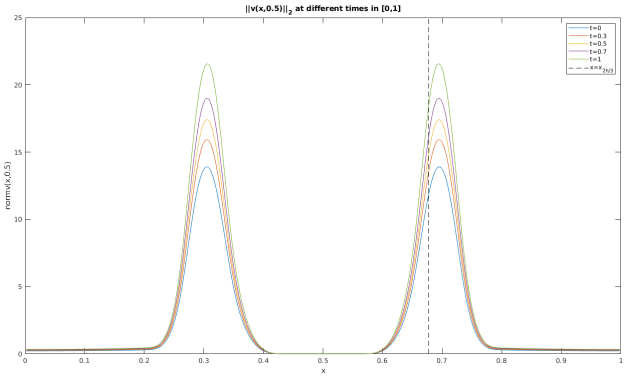

FIGURE 14. Plots of $\|v(x, 0.5, t)\|_2$ for $x \in [0, 1]$ and $t = 0, 0.3, 0.5, 0.7, 1$.

their maximum velocity at $z^* > \frac{2h}{3}$. In fact, in Figure 14 we observe that the maximum velocity is obtained at $x^* \approx 0.7 > x_{2h/3} = 0.6773$ where the maximum of the cell velocity norm is attained in the normal epithelium crypt, as it can be seen in Figure 8. In this scenario, cells continue to have an increasing velocity over the normal transit region defined by the quote $z = \frac{2h}{3}$ and, consequently, we have an expanded region for the proliferative transit cells. Biologically, the formation of an adenoma leads to the filling of the crypt walls following a bottom-up theory expansion [24, 25].

7. Conclusions

This paper deals with numerical tools for systems of partial differential equations defined by an elliptic equation and a parabolic equation of convection-diffusion-reaction type presenting mixed derivatives and a convective velocity depending on the gradient of the solution of the elliptic equation (1). Following the method of lines approach, we propose a finite-difference method for the IBVP (1) defined in nonuniform partitions of a two dimensional square and the stability and convergence analysis are provided.

In what concerns the stability of the semi-discrete approximation defined by the differential-algebraic IVP (11) we establish in Proposition 3.1 the first stability upper bounds that lead to the uniform boundness of the sequence of approximations for the pressure and concentration. After, in Proposition 3.3 we conclude the stability of the IVP (11).

The main convergence result is established in Theorem 4.4 which is consequence of a series of propositions where the particular structure of the spatial truncation error is exploited. In spite of the truncation error associated with

the pressure and concentration discretizations are only of first order, in Theorem 4.4 we show that the numerical approximations for the pressure and for the concentration are second order convergent with respect to a discrete H^1-norm. We observe that in [1] the authors studied a differential system analogous to the one studied here but where the elliptic equation does not depends on the solution of the parabolic equation and the last equation does not presents mixed derivatives. These two facts add difficulties in the construction of the numerical scheme as well as in its convergence analysis.

The numerical illustration of the convergence result is included in this paper. We also consider the numerical simulation of the cell dynamics in a colonic crypt in a normal and abnormal scenarios assuming that the density c of the semi-differentiated and stem crypt cells and the cell-cell adhesion pressure p responsible by its convective transport are solutions of the elliptic-parabolic IBVP (57) defined in a 3D surface representing a crypt. Taking into account that the 3D surface is a manifold, a differential-algebraic system of the type of the one studied here is obtained and then applying the numerical tool analyzed we illustrate the behavior of c, p and cell velocity v in normal and abnormal scenarios.

Acknowledgments

This work was partially supported by the Centre for Mathematics of the University of Coimbra - UIDB/00324/2020, funded by the Portuguese Government through FCT/MCTES.

References

[1] S Barbeiro, S. Bardeji, J A Ferreira, L Pinto, Non-Fickian convection-diffusion models in porous media, Numer Math 138, pp. 869–904, 2018.

[2] K E Brenan, S L Campbell, L R Petzold, Numerical Solution of Initial Value Problems in Differential-Algebraic Equations, Classics in Applied Mathematics, SIAM Philadelphia, 1995.

[3] B Dü̈ring, C Heur, High-order compact schemes for parabolic problems with mixed derivatives in multiple space problems, SIAM J Numer Anal 53, pp. 2113–2134, 2015.

[4] J A Ferreira, R Grigorieff, On the supraconvergence of elliptic finite difference schemes, App Numer Math 28, pp. 275–292, 1998.

[5] J A Ferreira, R Grigorieff, Supraconvergence and supercloseness of a scheme for elliptic equations on non-uniform grids, Numer Funct Anal Optim 27, pp. 539–564, 2006.

[6] G.C.M. Campos, Numerical analysis of multiscale methods for elliptic-parabolic problems with application in the cell dynamics during the formation of colorectal cancer. PhD Thesis, Universidade Estadual de Campinas, 2021.

[7] T Haentjens, K J in't Hout, ADI finite difference schemes for the Heston-Hull-White PDE, J Comp Fin 16, pp. 83–110, 2012.

[8] M N Koleva, L G Vulkov, A new mixed derivative terms removing numerical method for option pricing in the Heston model, AIP Conference Proceedings 2172, 070012, 2019.
[9] P Kunkel, V Mehrmann, Differential-Algebraic Equations - Analysis and Numerical Solution, EMS Textbooks in Mathematics, EMS Publishing House, Zürich, 2006.
[10] D V Guebel, N V Torres, A computer model of oxygen dynamics in human colon mucosa: Implications in normal physiology and early tumor develop- ment. J Theor Biol 250,pp. 389–409, 2008.
[11] I N Figueiredo and C Leal and G Romanazzi and B Engquist, Biomathematical Model for Simulating Abnormal Orifice Patterns in Colonic Crypts, Math Biosci, 315, 2019.
[12] I N Figueiredo and C Leal and G Romanazzi and B Engquist, Homogenization Model for Aberrant Crypt Foci, SIAM J Appl Math, 76, pp. 1152-1177, 2016.
[13] I N Figueiredo and C Leal and G Romanazzi and B Engquist and P N Figueiredo, A convection-diffusion-shape model for aberrant colonic crypt morphogenesis, Comput Visual in Sci,14, pp. 157-166, 2011.
[14] M. P. do Carmo, Differential geometry of curves and surfaces, 13, Inc.Englewood Cliffs, 1976
[15] E. P. Hsu, Heat Equations on Manifolds and Bismut's Formula, Stochastic Analysis and Partial Differential Equations: Contemporary Mathematics 429, American Mathematical Society, 2007.
[16] S.C.Brenner and L.Ridgway Scott, Convergent discrete Laplace-Beltrami operators over triangular surfaces, Geometric Modeling and Processing, 2004.
[17] I.M.M. van Leeuwen, H.M. Byrne, O.E. Jensen, J.R. King, Crypt dynamics and colorectal cancer: advances in mathematical modelling, Cell Prolif. 39, 157-181, 2006.
[18] F. A. Meineke, C. S. Potten and M. Loeffler, Cell migration and organization in the intestinal crypt using a lattice-free model, Cell Prolif, 34, 253-266, 2001.
[19] A. A. Almet, P. K. Maini, D. E. Moulton and H. M. Byrne, Modeling perspectives on the intestinal crypt, a canonical system for growth, mechanics, and remodeling. Current Opinion in Biomedical Engineering 15:32–39, 2020.
[20] D. Drasdo, M. Loeffler, Individual-based models to growth and folding in one-layered tissues: intestinal crypts and early development. Nonlinear Analisys 47, 245–256, 2001.
[21] C.S. Potten, M Kellett, S A Roberts, D A Rew, G D Wilson, Measurement of in vivo proliferation in human colorectal mucosa using bromodeoxyuridine, Gut, 33, 71-78, 1992
[22] C.S. Potten, C Booth, D.M. Pritchard, The intestinal epithelial stem cell: the mucosal governor. Int. J. Exp. Pathol. 78, 219, 1997.
[23] S. Lamprecht, A. Fich The cancer cells-of-origin in the gastrointestinal tract: progenitors revisited Carcinogenesis, 36, 8, 811–816, 2015.
[24] S.A. Lamprecht, Migrating colonic crypt epithelial cells: primary targets for transformation. Carcinogenesis, 23, 1777–1780, 2002.
[25] S.L. Preston, et al. Bottom-up histogenesis of colorectal adeno- mas: origin in the monocryptal adenoma and initial expansion by crypt fission. Cancer Res., 63, 3819–3825.

G.C.M. Campos
Institute of Mathematics, Statistics and Scientific Computing, State University of Campinas UNICAMP, Campinas, Brazil
E-mail address: geovan_carlos@hotmail.com

J. A. Ferreira
CMUC, Dep. of Mathematics, University of Coimbra, Portugal
E-mail address: ferreira@mat.uc.pt

G. Romanazzi
Dep. of Applied Mathematics, Institute of Mathematics, Statistics and Scientific Computing, University of Campinas, Brazil
E-mail address: roman@ime.unicamp.br